STRONG REAL-FLUID EFFECTS ON TRANSCRITICAL TURBULENT BOUNDARY LAYERS AT SUPERCRITICAL PRESSURES

Soshi Kawai

Department of Aerospace Engineering
Tohoku University
6-6-01 Aramaki-Aza-Aoba, Aoba-ku, Sendai, Miyagi 980-8579, Japan
kawai@cfd.mech.tohoku.ac.jp

ABSTRACT

Direct numerical simulation (DNS) of transcritical heated turbulent boundary layers on a zero-pressure-gradient flat plate at supercritical pressures is conducted by solving the full compressible Navier-Stokes equations. To the best of my knowledge, the present DNS is the first DNS of zero-pressure-gradient flat-plate transcritical turbulent boundary layer. The peculiar interactions between the strongly non-linear real fluid effect at the transcritical condition and wall turbulence, and their resultant turbulence statistics and turbulent kinetic energy budget are reported. The results indicate the importance of the compressibility effects (especially contribution of the pressure-dilatation) in the transcritical turbulent boundary layers even in a low Mach number condition. The analyses suggest that the compressibility effects originate from the abrupt variation in the density in the transcritical regime, which induce the significant expansion processes with a small temperature change through T_{pc} and causes the peculiar reduction of the Reynolds stresses at the transcritical condition.

INTRODUCTION

Understanding the physics of turbulent boundary layers at supercritical pressures and its turbulent heat transfer characteristics are crucial for many industrial applications, such as liquid rocket engines, supercritical steam generators in power plants, refrigerating systems with supercritical fluids, etc. Peculiar fluid behaviors in supercritical fluids occur within a narrow temperature range through the pseudo-critical temperature T_{pc} (shown in red dotted line in Fig. 1) where the specific heat at constant pressure c_p reaches its maximum value at a given pressure. Through the pseudo-critical temperature, the supercritical fluids behaves as liquid-like high-density fluid when the temperature $T < T_{pc}$ and vapor-like low-density fluid when $T > T_{pc}$ as shown in Fig. 2. The transition of thermodynamic and fluid transport properties from liquid-like fluid to vapor-like fluid through T_{pc} occurs continuously at a supercritical pressure, but varies significantly within a very narrow temperature range. We call this transitional condition, i.e., the abrupt and severe variation in fluid properties across T_{pc}, as "transcritical condition," and the transcritical turbulent boundary layer is the turbulent boundary layer at supercritical pressure where the transcritical condition exists within the boundary layer. Within the transcritical conditions, thermodynamic properties significantly deviate from
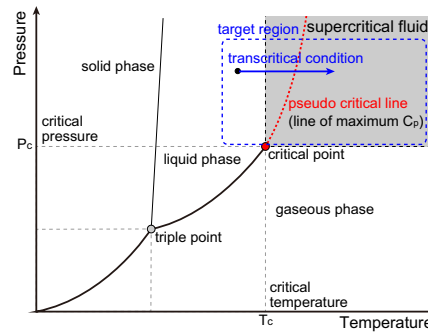

Figure 1. Transcritical condition through the pseudo-critical temperature in a phase diagram.
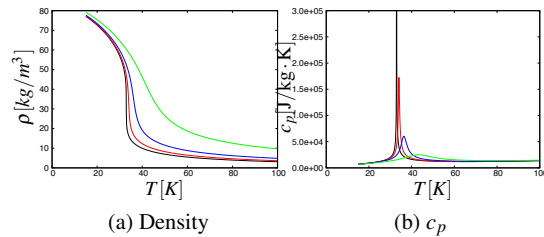

(a) Density (b) c_p

Figure 2. Variable thermodynamic properties for parahydrogen using REFPROP (NIST Standard Reference Database 23, Version 9.0). Density and specific heat in terms of the temperature at constant pressure. Black, $p = 1.2858$MPa; red, $p = 1.5$MPa; blue, $p = 2.0$MPa; green, $p = 4.0$MPa.

the perfect fluid due to the real fluid effects. Figure 2 shows the temperature dependency of density and c_p for parahydrogen under supercritical pressure conditions. Density, speed of sound, dynamic viscosity, and thermal conductivity decrease abruptly at the transcritical state while the specific heat at constant pressure c_p and specific heat γ increase rapidly and show a peak at $T = T_{pc}$. As shown in Fig. 2, these abrupt variations in fluid properties become less severe if the pressure increases.

Interestingly, experimental data show a significant change in turbulent heat transfer, which is one of the main interests in the engineering purpose (e.g., Yamagata *et al.* (1972)), when the transcritical condition, temperature through T_{pc}, exists within the boundary layers. However,

due to the severe high pressure conditions, it is extremely difficult to measure turbulence statistics and flow structures in the experiments.

Considering the present lack of understandings on the detailed turbulence statistics and flow structures in the transcritical turbulent boundary layers, direct numerical simulation (DNS) is an attractive choice. DNS is one of the most promising approach to elucidate the physics of the transcritical turbulent boundary layer and also to provide the detailed turbulence statistics and flow structures. However, because of the steep variation of the fluid properties in the transcritical real fluid effects through T_{pc}, a stable high-order accurate numerical simulation, which is required for high-fidelity numerical simulations such as DNS or large-eddy simulation (LES), becomes extremely difficult. Because of this difficulty in simulating transcritical flows, to the best knowledge of the author, there is only one DNS (even including LES) of the transcritical turbulent boundary layers by Bae *et al.* (2005, 2008) who studied transcritical turbulent vertical tube flows with buoyancy effects. However, Bae *et al.* (2005, 2008) employed a low-order accurate (second-order) scheme with a relatively coarse mesh resolution ($\Delta x^+ \approx 14.55$, $(R\Delta\theta)^+ \approx 9.14$) for their DNS. Also in their study, they neglected the compressibility effects by employing the low Mach number assumption.

In this study, DNS of transcritical heated turbulent boundary layers on a zero-pressure-gradient flat plate at supercritical pressure is conducted at a first time (to the best of my knowledge) by solving the full compressible Navier-Stokes equations. The motivation of this study is to elucidate the unsteady flow physics including the interactions between wall turbulence and abrupt variations of thermodynamic properties, and also provide reliable turbulence statistics. Target conditions are the transcritical conditions where the thermodynamic and fluid transport properties deviate significantly from the ideal fluid (i.e., within the blue dotted line in Fig. 1).

CHALLENGES IN TRANSCRITICAL SIMULA-TIONS

A significant challenge in simulating transcritical turbulent flows is to establish a numerical method that is robust to capture the steep variation of the thermodynamic properties through T_{pc}, while accurately resolving the broadband scales of turbulence. It is well known that if the steep variation of the thermodynamic properties is numerically captured in a strong conservative form using the total energy equation, spurious velocity and pressure oscillations are generated (Abgrall, 1996). This makes robust and accurate transcritical flow simulations extremely challenging.

Although the details of our proposed numerical method may be found in our publication (Kawai *et al.*, 2014), in this study, we derive the pressure evolution equation from the total energy equation, and directly solve the full compressible Navier-Stokes equations, the continuity, momentum, and pressure evolution equations (1), (2), and (3). Artificial density diffusion ($\nabla \cdot (\mathscr{A}_\rho)$) terms are introduced in a physically-consistent manner in order to capture the steep variation of thermodynamic properties in transcritical conditions robustly while preventing spurious velocity oscillations. Solving the pressure evolution equation allows us to prevent spurious pressure oscillations while employing an arbitrary equation of state including the present look-up table method.
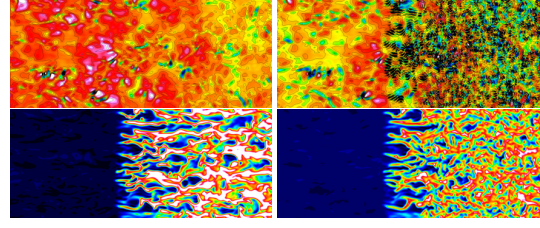
(a) Proposed method (b) Energy-based solver

Figure 3. Proposed method and conventional total-energy-based method on the DNS of heated transcritical turbulent boundary layer at supercritical pressure $p =$4MPa. Pressure contours (20 equally spaced contours in $3.8 \times 10^6 \leq p \leq 4.5 \times 10^6$ [MPa]) (on top) and temperature contours ($25 \leq T \leq 50$ [K]) (on bottom) in wall-parallel plane at $y^+ \approx 20$.

$$\frac{\partial \rho}{\partial t} + \nabla \cdot (\rho u) = \nabla \cdot (\mathscr{A}_\rho), \quad (1)$$

$$\frac{\partial \rho u}{\partial t} + \nabla \cdot (\rho u \otimes u + p\underline{\delta} - \underline{\tau}) = \nabla \cdot (\mathscr{A}_\rho u). \quad (2)$$

$$\frac{\partial p}{\partial t} + u \cdot \nabla p + \rho c_s^2 \nabla \cdot u - \frac{\alpha_p}{c_v \beta_t} \left[\frac{1}{\rho} \{ \underline{\tau} : \underline{S} - \nabla \cdot q \} \right] = 0, \quad (3)$$

$$\mathscr{A}_\rho = \chi_{\text{art}} \nabla \rho, \quad \chi_{\text{art}} = C_\chi \overline{\frac{c_s}{\rho} \left| \sum_{l=1}^{3} \frac{\partial^4 \rho}{\partial \xi_l^4} \Delta \xi_l^4 \Delta_{l,\chi} \right|}, \quad (4)$$

where the detailed notations may be found in Kawai *et al.* (2014). We have proved that solving this set of equations satisfies the physical velocity/pressure equilibrium through the abrupt variations of thermodynamic properties due to the transcritical condition, and thus enable robust and accurate simulations of transcritical flows (see Fig. 3; the present method is capable of simulating the transcritical flow without showing any spurious oscillations whereas the conventional total-energy-based method suffers from the unphysical pressure oscillations near the transcritical condition where the temperature goes through T_{pc}) (Kawai *et al.*, 2014).

In this study, by considering the deterioration of predictive accuracy by the existing equation of state models in the transcritical condition, the tabulated look-up table method is used to compute the thermodynamic and fluid transport properties. In this approach, by using the REFPROP database we first tabulate the thermodynamic and fluid transport quantities that are used to solve the employed governing equations 1, 2, and 3 (i.e., T, c_v, c_s, α_p, β_t, μ, and κ) (e.g., we store the thermodynamic and fluid transport quantities in the density and pressure parameter space with 2000×2000 data points to provide a sufficient number of data points in the transcritical condition). Then, with the tabulated look-up database the quantities are interpolated with a linear interpolation by using the density and pressure obtained by the governing equations 1 and 3 and used in the simulation.

The spatial derivatives in the governing equations are evaluated by the sixth-order compact differencing scheme (Lele, 1992), and eighth-order low-pass filter (Lele, 1992; Gaitonde & Visbal, 2000) is applied to the ρ, ρu, and p in order to ensure the numerical stability. The ex-

2

plicit third-order total variation diminishing (TVD) Runge-Kutta scheme []Shu & Osher (1988) is used for time integration. The time-step size used for the DNS of transcritical turbulent boundary layers is $dt * c_{s,\infty}/\delta_0 = 0.0004$ (the corresponding maximum inviscid Courant-Friedrichs-Lewy number is approximately 0.7).

RESULTS

DNS of transcritical heated turbulent boundary layers on a zero-pressure-gradient flat plate at supercritical pressure is conducted in this study to elucidate the unsteady flow physics including the interactions between wall turbulence and abrupt variations of thermodynamic properties, and also provide reliable turbulence statistics.

Flow Conditions and Computational Grids

In this study, parahydrogen is considered as a working fluid, which is relevant to the regenerative cooling propellant in liquid rocket engine applications. The low temperature ($T_\infty = 25K < T_{pc}$) fully-developed turbulent boundary layer is heated by the high-temperature wall ($T_w = T_{heat} = 100K$ and $200K > T_{pc}$), and thus because of the temperature condition $T_\infty < T_{pc} < T_{heat}$ the present DNS involves the transcritical condition where the temperature crosses T_{pc} within the boundary layer. Pressure is set to the supercritical pressure of $p = 2$MPa where the critical pressure for parahydrogen is $p_c = 1.28377$MPa. The two different pressure conditions give the different steepness of variation in the fluid properties as shown in Fig. 2. The computation uses a freestream Mach number of $M_\infty = 0.3$.

In the present DNS, two computational domains are run simultaneously, as illustrated in Fig. 4. The first domain (on the left in Fig. 4) is the unheated non-transcritical fully-developed turbulent boundary layer at supercritical pressure with the wall temperature $T_w = T_\infty = 25K$. This unheated domain is used as an inflow generator for the DNS of the transcritical heated turbulent boundary layer in the wall-heated domain (on the right in Fig. 4). The rescaling-reintroduction method Urbin & Knight (2001) is used to produce realistic inflow turbulence for the unheated domain with the recycling location taken as $12\delta_0$ downstream of the inflow (where δ_0 is approximately the 99% boundary layer thickness at $x = 10\delta_0$ in the unheated domain). Instantaneous flow at the location $x = 10\delta_0$ in the unheated domain is extracted and imposed as the inflow condition for the wall-heated domain (on the right in Fig. 4), in which the fully-developed turbulent boundary layer is heated by the high-temperature wall. In the domain of the transcritical turbulent boundary layer, the region of $0 \leq x/\delta_0 < 5$ remains unheated $T_w = T_\infty = 25K$, and the high-temperature wall condition ($T_w = T_{heat} = 100K$ and $200K$) is imposed in the region of $x/\delta_0 \geq 5$.

The computational test section for the unheated domain is $15\delta_0$, $2.4\delta_0$ and $6\delta_0$ in streamwise (x), wall-normal (y) and spanwise (z) directions, while additional large buffer regions with the length of $10\delta_0$ and $6.6\delta_0$ are placed at the outlet and upper boundaries to remove turbulent fluctuations and any reflections from the boundaries. The grid is smoothly stretched in the buffer regions toward the boundaries, thus coarsening the mesh toward the boundaries. The test section for the heated boundary layer extends to $30\delta_0$, $2.4\delta_0$ and $6\delta_0$ in x, y, and z directions, and the buffer regions with the length of $50\delta_0$ and $6.6\delta_0$ are placed at the outlet and upper boundaries. The wall boundary condition is
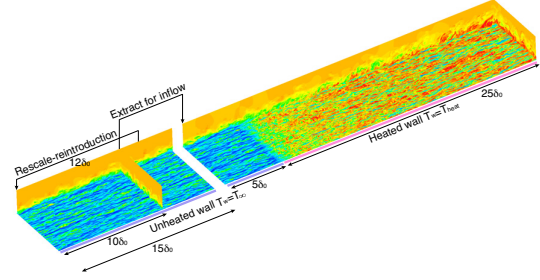

Figure 4. Direct numerical simulation of transcritical heated parahydrogen turbulent boundary layer on a zero-pressure-gradient flat plate under supercritical pressure conditions. Mach number contours in side, cross, and wall-parallel (at $y^+ \approx 20$) planes.

the isothermal non-slip condition, and the periodic boundary condition is imposed in the spanwise direction.

The Reynolds numbers at the inlet of the transcritical heated turbulent boundary layer (i.e., at $x = 10\delta_0$ in the unheated inflow generator domain) are $Re_\theta = \frac{\rho_\infty u_\infty \theta_0}{\mu_\infty} \approx 1,000$ and $Re_\tau = \frac{\rho_w u_\tau \delta_0}{\mu_w} \approx 400$ where $u_\tau = \sqrt{\tau_w/\rho_w}$. Note that Re_τ becomes relatively high compared to the value of Re_θ if one considers a turbulent boundary layer in an ideal fluid. This is because the dynamic viscosity is relatively low in the temperature region of $T < T_{pc}$ (liquid-like fluid region), and attains its minimum value at the pseudo-critical temperature T_{pc} due to the real fluid effects. The dynamic viscosity gradually increases with increasing the temperature at $T > T_{pc}$. Therefore, the Reynolds number based on the friction velocity becomes higher in the unheated non-transcritical boundary layer than the heated transcritical boundary layers.

The employed grid resolution in wall units is $\Delta x^+ = \Delta z^+ \approx 7.3$ and $\Delta y^+ \approx 0.23 - 7.3$ for the unheated condition at $T_w = T_\infty = 25K$. In the heated conditions, because of the increase in dynamic viscosity at $T > T_{pc}$, $\Delta x^+ = \Delta z^+ \approx 2.6$ and $\Delta y^+ \approx 0.08 - 2.6$ for $T_w = 100K$, and $\Delta x^+ = \Delta z^+ \approx 1.0$ and $\Delta y^+ \approx 0.03 - 1.0$ for $T_w = 200K$. The grid convergence study (although not shown here) indicates that the employed grid resolutions achieve the grid converged results.

Turbulence Statistics

Figure 5 shows the mean thermodynamic properties and velocity in the unheated non-transcritical and heated transcritical turbulent boundary layers at the supercritical pressures of $p = 2$MPa. The statistics of the heated transcritical cases are obtained at the location of $x = 25\delta_0$ in the transcritical heated computational domain (right domain in Fig. 4), and the unheated ($T_w = T_\infty = 25K$) results are obtained at $x = 10\delta_0$ in the unheated domain (i.e., equivalent to the inlet location in the transcritical heated domain).

Figure 5 shows the turbulence statistics of the unheated and heated turbulent boundary layers at the supercritical pressure of $p =2$MPa. Interestingly, although the heated turbulent boundary layers show significant density variations within the boundary layer because of the transcritical real fluid effects, the density weighted Van Driest transformation successfully collapses the mean velocity profile into the typical log-law that is obtained by the DNS of incompressible turbulent boundary layer with ideal gas law by Spalart (1988). The logarithmic region reduces by increasing the wall temperature because of the decrease in the local

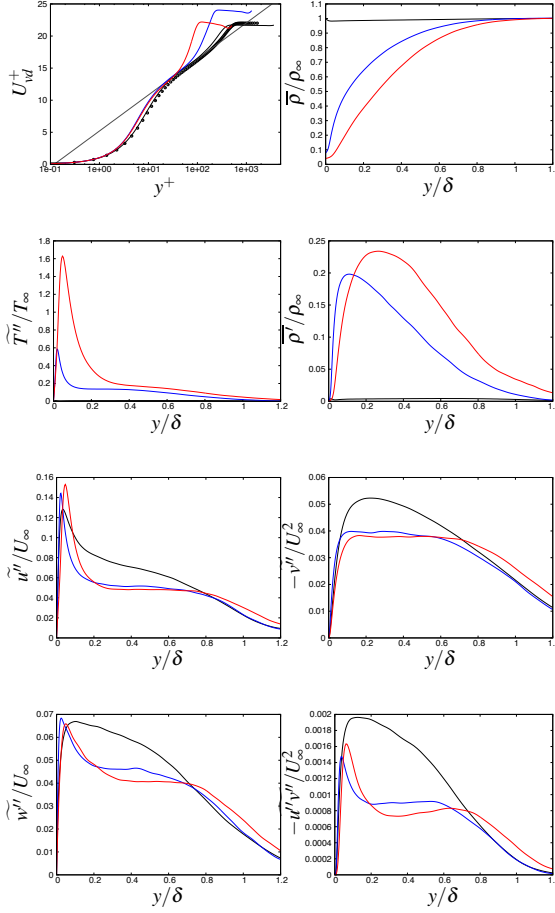Reynolds number Re_τ (i.e., the increase in the dynamic viscosity near the wall).

Figure 5. Turbulent statistics of unheated and heated turbulent boundary layers at supercritical pressure of $p = 2\,MPa$. Top, mean velocity and density; middle, thermodynamic fluctuations ($\widetilde{T''}, \overline{\rho'}$); bottom, Reynolds stresses ($\widetilde{u''}, -\widetilde{u''v''}$). Black, $T_w = T_\infty = 25K$; blue, $T_w = 100K$; red, $T_w = 200K$; circles in (a), incompressible DNS by Spalart at $Re_\theta = 1,410$ (Spalart, 1988); thin gray line in (a), $U^+_{vd} = 1/0.41\log(y^+) + 5.2$.

In the transcritical heated turbulent boundary layers, although the variance of the temperature $\widetilde{T''}$ shows a peak close to the wall (similar to the Reynolds normal stress $\widetilde{u''}$), the peak in the density fluctuations appears in the different locations, relatively away from the wall approximately at $y/\delta \approx 0.1$ for $T_w = 100K$ and $y/\delta \approx 0.25$ for $T_w = 200K$. This is unique phenomena in the transcritical turbulent boundary layers due to the strong real fluid effects. Since the density shows abrupt variation within a narrow temperature range through T_{pc} (see Fig. 2), the unique peak in the density fluctuations appears around the location where the temperature goes through T_{pc}. Interestingly, all the Reynolds stresses, $\widetilde{u''}$, $\widetilde{v''}$, $\widetilde{w''}$ and $-\widetilde{u''v''}$, significantly decreases around the location of the transcritical condition where the density fluctuations show a peak. Because of this

decrease in the Reynolds stresses the $-\widetilde{u''v''}$ and $\widetilde{w''}$ shows a peculiar peak near the wall, which has never been seen in ideal-fluid turbulent boundary layers.

In the unheated non-transcritical turbulent boundary layer, Van Driest transformed mean velocity and also all the Reynolds stresses closely agrees with the DNS of incompressible turbulent boundary layer with ideal gas law by Spalart Spalart (1988). These results suggest that even at the supercritical pressure condition if the flow is not in the transcritical condition (i.e., if the temperature does not go through the pseudo-critical temperature T_{pc}) the real fluid effects on the turbulent boundary layers are very limited.

Turbulent kinetic energy budget

In order to further investigate the turbulent boundary layers in the transcritical regime, the budget of the turbulent kinetic energy (TKE) $\widetilde{k} = \frac{1}{2}\widetilde{u''_i u''_i}$ is computed. The non-dimensionalized budget equation for TKE is

$$\frac{\partial \overline{\rho}\widetilde{k}}{\partial t} = -C + P + T + D_v + D_d + M + \Pi_d, \quad (5)$$

$$C = \frac{\partial}{\partial x_j}\left(\overline{\rho}\widetilde{u_j}\widetilde{k}\right), \quad P = -\overline{\rho}\widetilde{u''_i u''_j}\frac{\partial \widetilde{u_i}}{\partial x_j}, \quad (6)$$

$$T = -\frac{\partial}{\partial x_j}\left(\frac{1}{2}\overline{\rho}\widetilde{u''_i u''_i u''_j} + \overline{p'u'_j}\right), \quad (7)$$

$$D_v = \frac{M_\infty}{Re}\frac{\partial}{\partial x_j}\left(\overline{\sigma'_{ij}u'_i}\right), \quad D_d = -\frac{M_\infty}{Re}\overline{\sigma'_{ij}\frac{\partial u'_i}{\partial x_j}}, \quad (8)$$

$$M = \overline{u''_i}\left(\frac{M_\infty}{Re}\frac{\partial \overline{\sigma_{ij}}}{\partial x_j} - \frac{\partial \overline{p}}{\partial x_i}\right), \quad \Pi_d = \overline{p'\frac{\partial u'_i}{\partial x_i}}, \quad (9)$$

where C, P, T, D_v, D_d, M, and Π_d are the contributions due to convection, production, turbulent transport, viscous diffusion, energy dissipation, mass flux contribution associated to density fluctuations, and pressure dilatation, respectively. The mass flux contribution M and pressure-dilatation term Π_d in Eq. 9 are due to the compressibility effects. The equation is non-dimensionalized by ρ_∞, $c_{s,\infty}$, δ_0, and μ_∞, and $Re = \rho_\infty u_\infty \delta_0/\mu_\infty$ and $M_\infty = u_\infty/c_{s,\infty}$.

Figure 6 shows the TKE budget terms in the unheated non-transcritical and heated transcritical turbulent boundary layer ($T_w = 200K$) at $p = 2$ MPa. At the unheated non-transcritical condition, the main contributions are from P, T, D_v, and D_d, and the production and energy dissipation are balanced (i.e., the turbulence is in an equilibrium $P \approx D_d$) away from wall. The compressibility contributions (i.e., M and Π_d) on the TKE are negligible throughout the boundary layer due to the low Mach number condition. The budget terms in the unheated non-transcritical condition show similar profiles to the TKE budget obtained by incompressible turbulent boundary layer flows with the ideal gas law. At the heated transcritical condition, the features of P, T, D_v, and D_d are similar to the unheated non-transcritical condition (although in some parts near the wall the negative contributions of the turbulent transport T and viscous diffusion D_v exceed the energy dissipation D_d). On the other hand, the contributions of the compressibility effects drastically change: both the mass flux contribution M and pressure-dilatation Π_d terms are not negligible anymore in the heated transcritical condition even in this low Mach number condition.

The mass flux contribution M due to the increase in the density fluctuations in the transcritical abrupt variation in the density has a positive contribution to the TKE.

(a) Non-transcritical
condition, $T_w = T_\infty = 25K$

(b) Transcritical condition,
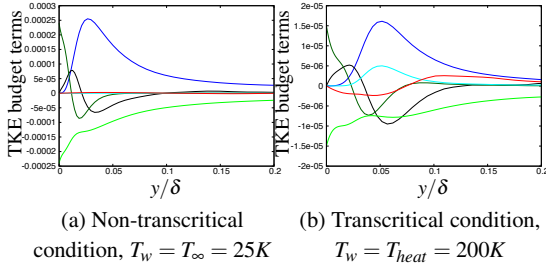$T_w = T_{heat} = 200K$

Figure 6. Turbulent kinetic energy budget in unheated non-transcritical and heated transcritical turbulent boundary layers at supercritical pressure of $p = 2$ MPa. Blue, production P; black, turbulent transport T; dark green, viscous diffusion D_v; light green, energy dissipation D_d; cyan, mass flux contribution M; red, pressure dilatation Π_d.

The pressure-dilatation Π_d term has a negative contribution near the wall where the Reynolds stress components start to damp and show a peculiar peak in $\widetilde{w''w''}$ and $-\widetilde{u''v''}$ (see Fig. 5). This suggests that the compressibility contribution, especially the pressure-dilatation term, possibly plays an important role in the Reynolds stress reduction in the transcritical regime shown in Fig. 5. Away from the wall, Π_d then turns to a positive contribution to the TKE. The transcritical condition at $T_w = T_{heat} = 200K$ clearly shows that the turbulence is in a non-equilibrium state (i.e., $P \neq D_d$) away from the wall, and the pressure dilatation plus production and the energy dissipation are balanced (i.e., $P + \Pi_d \approx D_d$).

Instantaneous Flowfields

Figure 7 shows instantaneous snapshots of the heated transcritical transcritical boundary layer in the wall-parallel planes at $y/\delta \approx 0.05$ at $p = 2$MPa and $T_w = 200K$ condition. The region of the square boxes with black solid line in Fig. 7 is zoomed in and shown with the velocity fluctuation vectors in Fig. 8. The location of $y/\delta \approx 0.05$ corresponds to the location where the pressure-dilatation term attains its maximum.

It is clear that the instantaneous Reynolds shear stress starts to decrease and the density fluctuations start to increase in the streamwise location where the low-temperature fluid is heated by the high-temperature wall and the local temperature goes through T_{pc}. These instantaneous features qualitatively agree with the turbulence statistics discussed in the turbulence statistics. Since c_p reaches its peak value at $T \approx T_{pc}$, the filaments of high c_p value indicate the location of the transcritical condition where $T \approx T_{pc}$. The high c_p filaments present along the edge between the low-temperature fluid and the heated high-temperature fluid. The low-temperature high-density fluid is entrained from the higher potion of the boundary layer by the turbulence, and thus the low-temperature regions and high velocity fluctuation regions show a good correlation.

Regarding the pressure-dilatation term Π_d that is not negligible in the transcritical conditions, significant divergence of velocity fluctuation clearly appears in the heated transcritical regions at $y/\delta \approx 0.05$ (where Π_d attains its maximum and has a negative impact to the TKE). Considering that the pressure fluctuations are somewhat reduced in the transcritical heated region, the major contrition to Π_d is the divergence of velocity fluctuation. Also note that the no-

(a) $25 \leq T \leq 150$ [K]

(b) $1.0 \leq c_p \leq 4.0$ [10^4 J/kg·K]

(c) $-0.5 \leq \rho'/\rho_\infty \leq 0.5$

(d) $-0.005 \leq -\widetilde{u''v''}/u_\infty^2 \leq 0.015$

(e) $-0.5 \leq \frac{\partial u_i}{\partial x_i}\frac{\delta_0}{u_\infty} \leq 0.5$

(f) $-1.0 \leq p'/\rho_\infty c_{S,\infty}^2 \leq 1.0$ [$\times 10^{-3}$]
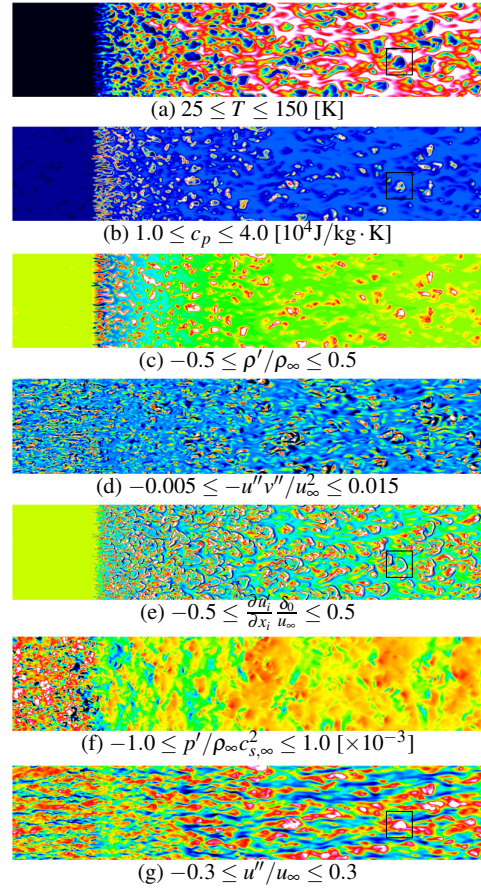
(g) $-0.3 \leq u''/u_\infty \leq 0.3$

Figure 7. Instantaneous snapshots of the transcritical heated boundary layer in wall-parallel planes at $y/\delta \approx 0.05$ in the region of $0 \leq x/\delta_0 \leq 30$ and $0 \leq z/\delta_0 \leq 6$ (whole right-side domain in Fig. 4) under $p = 2$MPa and $T_w = 200K$ conditions.

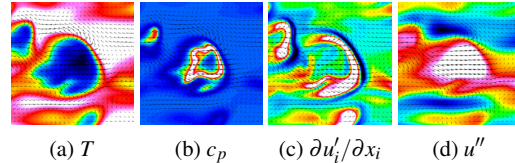(a) T (b) c_p (c) $\partial u_i'/\partial x_i$ (d) u''

Figure 8. Zoomed instantaneous snapshots overlaid with velocity fluctuation vectors (every third grid point) in the region of the black solid-line boxes in Fig. 7.

ticeable divergence of velocity fluctuation presents without shock waves in the flow. The pressure fluctuation contours are smooth, and the turbulent Mach number is low enough not to generate shock waves. Therefore, the flow is basically in the incompressible regime, but the non-linear behaviors of thermodynamic properties due to the real fluid effects in the transcritical flow lead the non-zero divergence of velocity fluctuation.

Closely looking into the region of the divergence of velocity fluctuation (see Fig. 8), the bow-shaped $\frac{\partial u_i'}{\partial x_i}$ consists of the strong expansion followed by the compression in the streamwise direction. The strong expansion region exists along $T > T_{pc}$ region as to surround the high c_p filament (i.e., the region of the transcritical condition where

$T \approx T_{pc}$). This phenomenon can be interpreted as that the $T > T_{pc}$ region next to the high c_p filament is considered to be the region where the low-temperature fluid $T < T_{pc}$ is heated and the temperature goes through T_{pc}, and thus the density decreases abruptly in this region. Considering the mass flux conservation, this region becomes a strong expansion region (i.e., positive divergence region) due to the peculiarity of the transcritical condition due to the strongly non-linear real fluid effects. This expansion process is considered to occur rapidly within a narrow temperature range. Although we need further investigations, it is reasonable to conclude that the appearance of the pressure-dilatation term is because of this strong expansion process due to the strongly non-linear behaviors of thermodynamic properties in the transcritical condition. These results also indicate the importance of solving the full compressible Navier-Stokes equations (i.e., without the low Mach number assumption that was used in the study of Bae *et al.* (2005, 2008) in order to understand the physics of transcritical turbulent boundary layer where the compressibility effects are not negligible.

CONCLUSIONS

DNS of transcritical heated turbulent boundary layers on a zero-pressure-gradient flat plate at supercritical pressures was conducted by using a numerical strategy that is robust and high-order accurate for enabling to simulate transcritical flows at supercritical pressure with the abrupt variations in thermodynamic properties due to the strong real fluid effects. To the best of my knowledge, the present DNS is the first DNS of zero-pressure-gradient flat-plate turbulent boundary layer at transcritical conditions. The unique and interesting interactions between the real fluid effects at the transcritical conditions and wall turbulence, and their turbulence statistics, which have never been seen in the ideal-fluid turbulent boundary layers, were discussed. We also addressed the impact of the transcritical real fluid effects on the turbulent kinetic budget, and the results suggest the importance of compressibility effects (especially, pressure-dilatation correlation) on the turbulence statistics

in the transcritical turbulent boundary layers even in a low Mach number condition (i.e., without shock waves).

REFERENCES

Abgrall, R. 1996 How to prevent pressure oscillations in multicomponent flow calculations: A quasi conservative approach. *Journal of Computational Physics* **125** (1), 150–160.

Bae, J. H., Yoo, J. Y. & Choi, H. 2005 Direct numerical simulation of turbulent supercritical flows with heat transfer. *Physics of Fluids* **17** (10), 105104.

Bae, J. H., Yoo, J. Y. & McEligot, D. M. 2008 Direct numerical simulation of heated co_2 flows at supercritical pressure in a vertical annulus at $re = 8900$. *Physics of Fluids* **20** (5), 055108.

Gaitonde, D. V. & Visbal, M. R. 2000 Padé-type higher-order boundary filters for the Navier-Stokes equations. *AIAA Journal* **38** (11), 2103–2112.

Kawai, S., Terashima, H. & Negishi, H. 2014 A robust and accurate numerical method for transcritical turbulent flows at supercritical pressure with an arbitrary equation of state. *submitted to Journal of Computational Physics* .

Lele, S. K. 1992 Compact finite difference schemes with spectral-like resolution. *Journal of Computational Physics* **103** (1), 16–42.

Shu, C. W. & Osher, S. J. 1988 Efficient implementation of essentially nonoscillatory shock capturing schemes. *Journal of Computational Physics* **77** (2), 439–471.

Spalart, R. P. 1988 Direct simulation of a turbulent boundary layer up to r_θ=1410. *Journal of Fluid Mechanics* **187**, 61–98.

Urbin, G. & Knight, D. 2001 Large-eddy simulation of a supersonic boundary layer using an unstructured grid. *AIAA Journal* **39** (7), 1288–1295.

Yamagata, K., Nishikawa, K., Hasegawa, S., Fujii, T. & Yoshida, S. 1972 Forced convective heat transfer to supercritical water flowing in tubes. *International Journal of Heat and Mass Transfer* **15** (12), 2575–2593.